PROCEEDINGS, 44th Workshop on Geothermal Reservoir Engineering
Stanford University, Stanford, California, February 11-13, 2019
SGP-TR-214

Preliminary Geochemical Model of the Domo San Pedro Geothermal Field in San Pedro Lagunillas, Mexico

Esteban Rodriguez, Fernando Ocampo, Violeta Reyes, David Ávalos, Julio García

Km 12 Carr. Chapalilla-Compostela. San Pedro Lagunillas, Nayarit. Mexico

ejrodriguezpi@gdragon.com.mx

Keywords: geochemistry, geochemical model, Domo San Pedro, mixing models, conceptual model

ABSTRACT

Domo San Pedro is a magmatic hydrothermal system located in San Pedro Lagunillas, Nayarit. The Domo San Pedro reservoir is a liquid-dominated type of reservoir, which is evident in the fact that the pressure and temperature profiles of the wells show that in the reservoir the pressure is hydrostatic, meaning higher than the saturation pressure which makes compressed liquid the prevailing conditions. Also, the wells discharge a mix of brine and steam. The water classification of the field is type sodium chloride, with a neutral or slightly acidic pH. The chloride concentration in the reservoir varies between 850 ppm to 1200 ppm. Brine geothermometer temperatures agree well with downhole surveys and show the field has a temperature between 260°C and 340°C. By combining the chemistry observed from the wells and the warm springs, with a structural geology campaign, a preliminary origin of fluid and flow direction, as well as a geochemical model is presented here.

1. DOMO SAN PEDRO GEOTHERMAL PROJECT

1.1 Geological Overview

The Domo San Pedro (DSP) geothermal field is in the state of Nayarit, to the West of Mexico. The topography ranges from 1800 m a.s.l. on top of the Domo San Pedro, to 800 m a.s.l. The DSP project is part of a silicic volcanic complex with the most recent activity 100,000 years ago. The most recent volcanism is represented by an alignment of numerous silicic and monogenetic cinder cones in a NNW-SSE direction (Figure 1) with a WNW-ESE alignment to the north of monogenetic volcanoes and the Ceboruco stratovolcano (~0.045Ma).

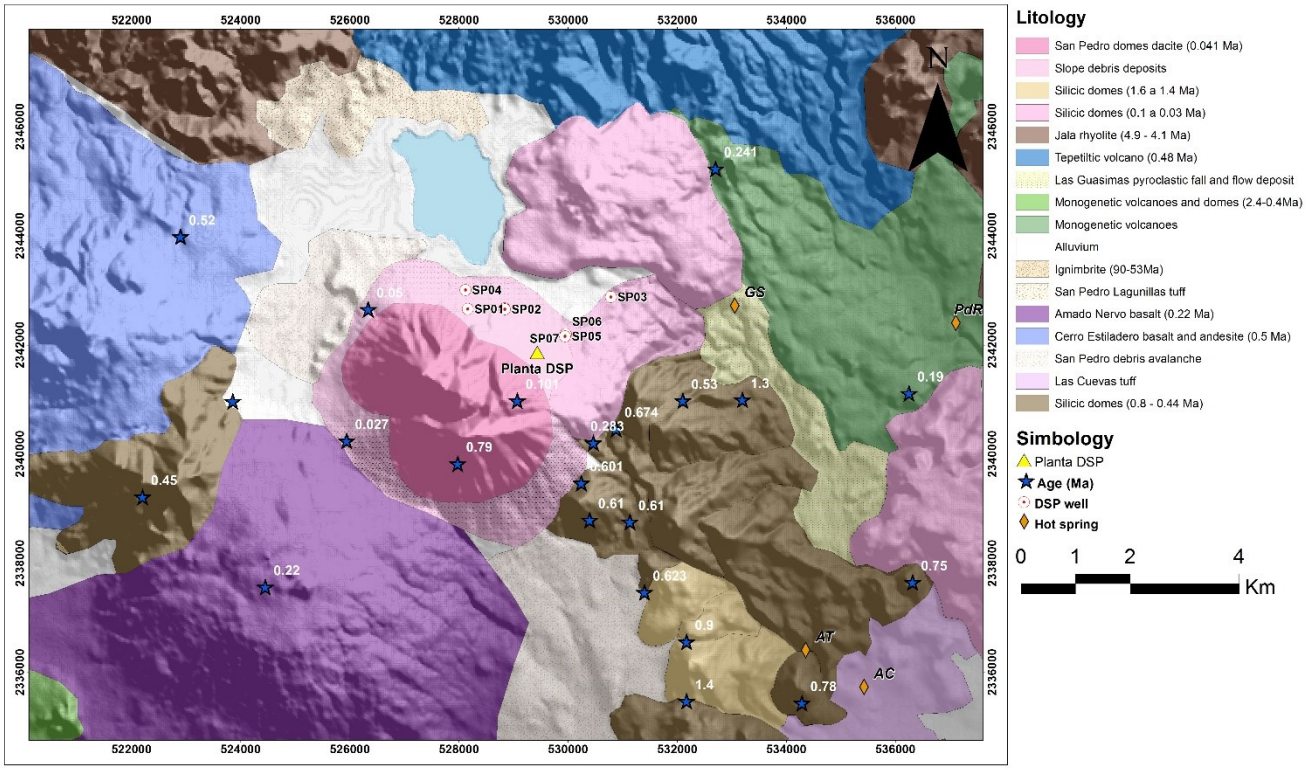

Figure 1: Geologic map showing local geology, geothermal wells and warm spring discharges.

The San Pedro region is localized inside the Compostela Graben and inside a depression caused by faults in N-S, NE-SW, NW-SE and E-W directions. It's a complex and asymmetric depression formed during the middle Miocene to Pliocene with a vertical displacement that exceeds 2 km.

The Compostela graben is formed by two faults: CP fault (NW 137° SE) and PD Fault (NW 319° SE) which limit the 10 km wide depression. This NW-SE fault system is part of the same structural trend and outcrop in the zone as the CP, SP, CF, CB and AJ faults, and are important because they have the same orientation as the regional graben. The Southeastern section faults CF, CB and AJ are found, the latter one being a discharge medium of the reservoir, evident in the AT and AC warm springs.

The N-S faults of the middle Miocene reactivated during the Pliocene, and NE-SW faults serve as the reservoir's limit. The eastern flanks of the domic complex are limited by a NE-SW fault, named LL, with a dip towards the Southeast, in the direction of the AC and AT warm springs.

Trending E-W faults are also present and are frequent. They are considered to be a secondary system derived from the dominant NW-SE extensional regime from the Pliocene. These faults become relevant because the cut the northern flank of the Domo San Pedro and outcrop as OC, AV and GS faults. The GS and PdR warm springs are associated to these faults.

1.2 Geothermal Wells and Warm Springs Overview

The Domo San Pedro geothermal field has nine geothermal wells, four of which are production wells and one of which is a reinjection well. The rest have been used intermittently as reinjection wells or monitoring wells. The wells are distributed in an E-W manner alongside the Northern flank of the domes. Most warm springs discharge to the East and Southeast of the domic complex. The only exception is AN, which is found to the South of the field. GS and PdR discharge to the East of the filed and AT and AC to the Southeast.

Accurate records of the chemistry of the wells and warm springs began in 2016, when a quarterly sampling program was put in place. The sampling of geothermal wells follows the general guidelines of Ármansson and Ólaffson (2007), Arnorsson, et al, (2006) and Marini (2000). A Webre type separator is used to separate the liquid and steam phases at discharge. The warm spring discharges are sampled by a third-party laboratory due to a legal requirement.

2. CHEMICAL RESULTS

Table 1: Composition of Warm Springs around Domo San Pedro

Warm Spring	Flow (L/min)	Elevation (m)	Temp (°C)	pH (20°C)	Li	Na	K	Ca	Mg	SiO_2	B	Cl	F	SO_4	HCO_3	CO_3	NH_4	As	Ba	Fe	Mn	Cond. µS/cm
					Concentrations (mg/kg) for water collected at atmospheric pressure from discharge																	
GS	374	1056	30.86	6.81	0.6	98.4	10.3	18.6	13.5	94.6	3.2	113.4	0.4	< 10.3	190.9	< 5.0	< 0.2	0.1	0.1	0.0	< 0.05	780.4
PdR	660	845	29.57	6.68	0.2	71.8	5.6	13.0	11.5	112.7	1.7	72.3	0.3	27.1	120.2	< 5.0	< 0.2	0.1	< 0.5	0.1	< 0.05	493.4
AT	376	789	38.00	7.29	0.3	70.9	7.6	12.0	11.6	115.5	1.9	60.5	0.3	< 10.3	191.9	< 5.0	< 0.2	0.1	0.1	0.0	0.1	561.1
AC	26	764	44.14	7.06	0.4	93.0	10.4	11.4	13.1	123.6	2.8	105.2	0.4	< 10.3	198.4	< 5.0	< 0.4	0.1	0.1	0.0	< 0.05	760.3
AN	53	782	36.43	7.24	0.3	68.3	7.7	7.6	5.6	132.7	1.6	58.5	0.3	10.7	140.8	< 5.0	< 0.2	0.2	0.1	3.4	0.0	471.9
SI	29.5	790	38.86	7.80	0.1	145.6	4.1	4.4	2.5	73.3	1.6	151.1	0.4	74.5	112.1	< 5.0	< 0.2	0.0	0.1	0.1	0.0	940.0
RSP	65	1309	22.71	7.24	0.0	9.7	3.6	3.1	0.8	46.3	0.1	13.1	0.2	13.6	49.7	< 5.0	0.2	0.0	< 0.5	0.9	0.0	767.0
LSP	-	1250	24.43	8.50	0.0	34.9	27.4	7.5	7.6	8.4	0.1	26.0	0.4	< 10.3	139.6	35.5	0.1	0.0	0.1	0.2	0.1	371.9

Table 2: Isotopic Composition of Warm Springs and Precipitation around DSP

Warm Spring	Elevation (m)	Season	Temp (°C)	del ^{18}O (‰)	del D (‰)	Season	Temp (°C)	del ^{18}O (‰)	del D (‰)
GS	1056	Dry	30.1	-7.10	-52.30	Wet	29.1	-7.02	-53.06
PdR	845	Dry	28.1	-8.50	-60.30	Wet	28.4	-8.60	-60.79
AT	789	Dry	38.5	-6.70	-52.50	Wet	38.7	-7.18	-54.09
AC	764	Dry	46.3	-7.40	-55.90	Wet	46.3	-7.59	-57.80
AN-1	782	Dry	35.5	-8.10	-60.20	Wet	37	-8.43	-60.90
AN-2	780	Dry	37.9	-8.30	-60.20	-	-	-	-
SI	790	Dry	39.9	-7.90	-55.80	Wet	39.9	-8.08	-57.17
RSP	1309	Dry	14.9	-8.60	-59.50	Wet	22.9	-8.70	-59.43
LSP	1250	Dry	22.0	0.90	-5.10	Wet	25.2	-0.81	-16.95
RST	850	Dry	28.3	-8.20	-57.90	Wet	22.4	-8.36	-58.40
RAM	323	Wet	27.4	-7.59	-57.04	Dry	24.6	-7.29	-53.77
RCH	312	Wet	29.9	-7.70	-54.38	-	-	-	-
LTT	1417	Wet	21.8	-2.95	-35.06	-	-	-	-
LSM	740	Wet	29.7	1.75	-7.40	-	-	-	-
PLG	805	Dry	31.6	-8.63	-62.45	-	-	-	-
PAD	1277	Dry	23.7	-7.90	-56.00	-	-	-	-
ULB	853	Dry	29.3	-8.43	-59.91	Wet	27.4	-8.33	-59.38
BP5	873	Dry	28.8	-8.31	-57.35	Wet	26.7	-8.35	-57.79
PDS-1	1270	Dry	25.1	-8.55	-60.50	-	-	-	-
PEG	1312	Dry	30.5	-8.85	-61.73	-	-	-	-
PDS-2	1271	Dry	25	-8.51	-60.18	-	-	-	-
PLL	1268	Dry	25.5	-8.38	-59.75	-	-	-	-
UAN	879	Dry	27	-8.01	-54.92	Wet	24.8	-7.89	-54.17
ESP	884	Dry	24.1	-7.51	-51.80	Wet	25	-7.69	-51.99
RAM	323	Wet	25.6	-7.37	-50.97	-	-	-	-
PEG	1312	Wet	27.8	-8.75	-61.46	-	-	-	-
Precipitation	1278	-	-	-10.5	-72.5	-	-	-10.1	-68.6
Precipitation	1276	-	-	-7.68	-49.92	-	-	-8.69	-56.81
Precipitation	1276	-	-	-9.27	-63.39	-	-	-	-

Table 3: Chemical Composition of Brine at Separation Pressure of Production Wells at DSP

Well	del ^{18}O	del D	pH	Li	Na	K	Ca	Mg	SiO_2	B	Cl	SO_4	HCO_3	NH_4	As	Rb	Fe	Al	Cond.
	(‰)	(‰)		Concentrations (mg/kg) for water collected at separator pressure															µS/cm
SP01	-5.94	-54.14	5.98	14.3	761.7	279.1	3.8	0.05	1242.2	44.4	1533.2	9.9	6.01	1.76	0.74	2.38	0.01	0.33	4733
SP04	-6.13	-55.71	6.88	13.9	757.6	255.1	8.4	0.02	986.9	45.8	1488.6	19.3	42.21	2.34	4.32	2.39	0.04	0.52	4610
SP05	-5.71	-54.87	6.48	11.9	867.9	252.6	17.7	0.04	751.5	52.5	1658.4	20.6	41.91	3.79	6.40	3.00	0.00	0.16	5192
SP06	-5.79	-54.02	6.56	6.9	670.8	102.6	8.1	0.07	543.3	42.3	1214.9	28.2	31.83	3.54	0.05	1.09	0.02	0.53	3746

Table 4: Non-Condensable Gases at Separator Pressure Conditions for Production Wells at DSP

Well	Total Gas	He	H2	Ar	N2	O2	CH4	CO2	H2S	NH3
	Concentrations (wt%) for steam collected at separator pressure									
SP01	0.852%	0.00020%	0.032%	0.043%	1.042%	0.000%	0.006%	90.060%	8.804%	0.016%
SP04	1.060%	0.00027%	0.016%	0.023%	0.744%	0.000%	0.010%	92.430%	6.737%	0.038%
SP05	2.034%	0.00013%	0.036%	0.040%	1.364%	0.000%	0.007%	93.270%	5.273%	0.014%
SP06	1.873%	0.00014%	0.033%	0.035%	1.273%	0.000%	0.006%	94.062%	4.564%	0.024%

3. INTERPRETATION OF WARM SPRING RESULTS

This section focuses on the physical and chemical characteristics of the springs around Domo San Pedro and analyzes this information to draw conclusions about the underlying flow of hot brine.

3.1 Molecular Ratios

From a graph correlating the concentrations of Boron and Chlorides of the warm springs around the field, Figure 2, it's clearly visible the strong correlation between GS, AC, PdR, AT and AN, leaving SI alienated from this tendency. Given how groundwater dilution will dilute all solutes in the same manner, this suggests that SI belongs to a different reservoir and that the other warm springs share a same origin but have been diluted in different proportions. Also, this figure shows that AT, PdR and AN gather around the same region of the graph, while AC and GS have higher concentrations of Boron and Chlorides and plot closer together. The molecular ratio Cl/B, B/Li and HCO_3/SO_4 are shown in Table 5. This tables shows that overall, the Cl/B ratio of all the thermal waters discharging around DSP is very similar, suggesting a common source reservoir. This ratio does not need to be identical to suggest a common source reservoir, as Boron can be induced by a change in lithology at depth over a field or by adsorption onto clays during lateral flow, as Nicholson (2012) mentions. Furthermore, if the reservoir is very homogeneous, this would suggest that GS and AC have been diluted the least, owing to their higher Cl and B concentrations. This, however, is not reflected in their temperatures as they are not both the hottest springs, which may signal that GS has been conductively cooled to some degree. Also, as Cl/B tends to decrease with flow direction, this suggests that the flow tends to the SE of the field, towards the direction of AT and AC. As the fluid flows away from the upflow, it has time for water-rock reactions that increase the bicarbonates and decrease the sulfates, which gives higher HCO_3/SO_4 ratios. This tendency is clear as the higher HCO_3/SO_4 ratios toward the SE, supporting that the fluid flow is in this direction. See Figure 1 for the location of all warm springs around the field.

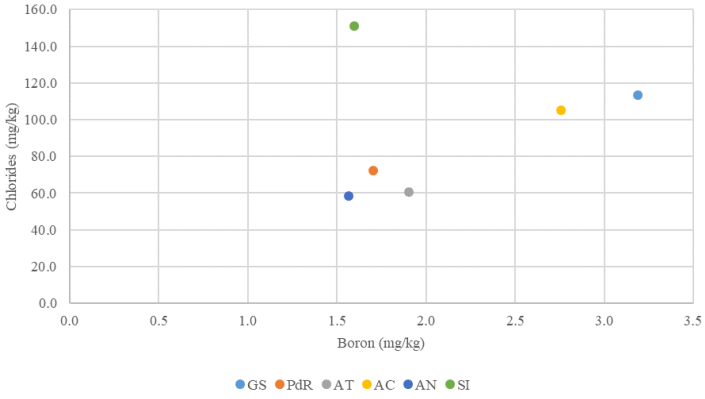

Figure 2: Cl/B correlation for warm springs around Domo San Pedro

Table 5: Molecular ratios for warm springs around DSP

Warm Spring	Cl/B	B/Li	HCO3/SO4
GS	10.85	3.17	> 29.24
PdR	12.96	4.47	6.98
AT	9.68	4.51	> 29.40
AC	11.63	4.07	> 30.39
AN	11.39	3.20	20.80
SI	28.86	8.96	2.37

3.2 Ternary Diagrams of Warm Springs' Discharges at DSP

Figure 3, from Powell and Cumming (2010), presents the Cl-SO_4-HCO_3 diagram for the Domo San Pedro geothermal system, where it can be seen how GS, PdR, AT, AC and AN cluster around the same peripheral water region, while SI is separate and plots near the middle of the diagram. This further supports the idea that SI belongs to a different geothermal system and has been subject to different mixing dynamics relative to the rest of the warm springs. Plotted in the same diagram for reference are the data points for LSP, RSP and all 6 geothermal production wells. Also, this diagram provides an initial indication of mixing relationships between mature, reservoir waters, and the warm springs plotted.

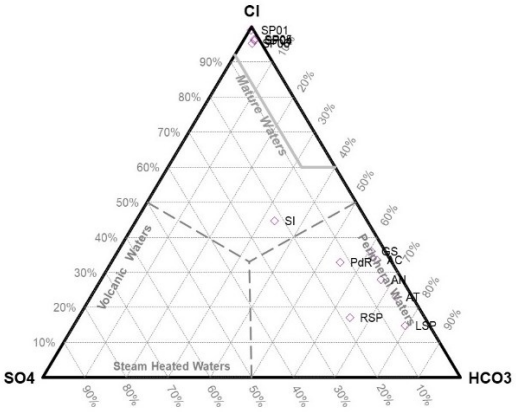

Figure 3: Cl-SO4-HCO3 Ternary Diagram for Thermal Springs – DSP

Figure 4 from Powell and Cumming (2010), is a Li-Cl-B ternary diagram showing the similarities among GS, PdR, AT, AC and AN. The tightly clustered warm springs in this diagram again supports the idea that they arise from a common reservoir, as discussed before. SI once again plots separate from the rest of warm springs. LSP and RSP are plotted for reference, as well as all geothermal production wells.

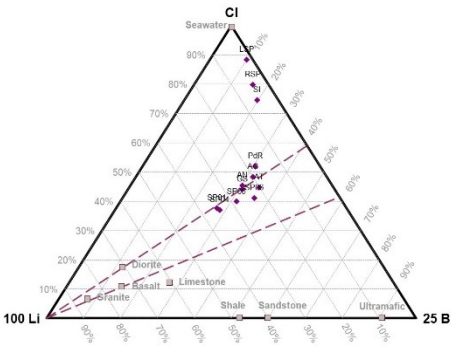

Figure 4: Li-Cl-B Ternary Diagram for Warm Springs - DSP

Figure 5 from Powell and Cumming (2010), shows the Na-K-Mg ternary diagram. All the warm springs are plotted very close together, making it essentially impossible to distinguish one from the other. However, an approximate trend line can be drawn from this figure (red line), suggesting equilibrium temperatures for the warm springs around 260°C. This agrees with estimated reservoir temperatures obtained via silica mixing model, as will be shown in subsequent sections.

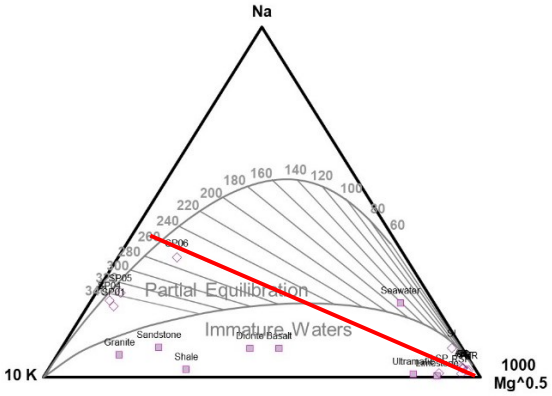

Figure 5: K-Na-Mg Ternary Diagram for Warm Springs - DSP

3.3 Enthalpy-Silica Mixing Model

The Enthalpy – Silica Mixing Model is a technique proposed by Fournier (1977) to estimate the temperature of the hot water component of different warm springs. Owing to the low temperatures seen in the springs around Domo San Pedro and considering the relatively large quantity of silica relative to the discharge temperature, it has been assumed that the procedure to follow corresponds to the scenario where there has been steam or heat loss before mixing.

Table 6 summarizes the results of applying this mixing method for all the warm springs around DSP. The only warm spring where this model cannot be applied is PdR due to a discrepancy between the silica content of PdR and its temperature. In other words, for the silica content it is discharging, the temperature should be higher, signaling a possible subsurface process that has not been considered, perhaps conductive cooling. Table 6 also provides a comparison of estimated temperatures by geothermometers, and Silica Mixing Model and it shows coherence between the Na/K geothermometer, and temperatures estimated by the Silica Mixing Model for all surrounding warm springs, except for SI, supporting further the idea that this spring lies in a different geothermal field. Because the parent fluid fraction of PdR was impossible to calculate with the Silica Mixing Model, a mass balance equation was solved for the fraction of geothermal water that could be reasonably expected to be discharged at this spring given the discharge chloride concentration, estimated reservoir chlorides and total flow. It's worth pointing out that this procedure assumes that steam separation occurs at 100°C and 1atm. If steam was lost at higher temperature, it would be necessary to use an intermediate curve, between the maximum steam loss and quartz solubility curve.

Also following Nicholson (2012), it is possible to estimate the fraction of parent fluid in the spring water (after steam loss) and the fraction, by weight, of original fluid lost as steam before mixing. It was found that GS has 14% parent fluid component, 22% for AT, 30% for AC, 21% for AN and 24% for SI. Because the model seems to not be applicable for PdR, it's impossible to estimate a fraction of hot water component for this spring. Regarding weight fraction of fluid lost as steam, it can be seen in Table 6 that GS, AT, AC and AN have lost around 30% of mass. The parent fluid fraction points to the fluid flow being towards the SE of the field supporting what has been discussed from the Cl/B and HCO_3/SO_4 ratios. Finally, the fluid lost as steam seams to point to all the warm springs boiling at around the same pressure and temperature. It's also worth mentioning that this mixing model was done graphically and not analytically, so this information has a margin of error and all the fractions and temperatures calculated should be considered as a range and not a fixed value. However, the small error should not change the general conclusions of this analysis.

Table 6: Comparison of Geothermometry Temperatures and Mixing Models

Warm Spring	T_{QTZ} max loss (°C)	T_{NAK} (°C)	$T_{SiO2\ model}$ (°C)	Parent Fluid Fraction	Fluid Lost as Steam
GS	130.3	219.7	248.9	14%	33%
PdR	138.6	197.6	-	6%*	-
AT	139.7	220.8	227.8	22%	29%
AC	146.2	224.9	214.9	30%	25%
AN	146.6	225.1	244.7	21%	32%
SI	118.8	132.6	197.3	24%	22%

* Calculated with a mass balance of the estimated chloride concentration in the reservoir (1000ppm) and chlorides observed at discharge

4. INTERPRETATION OF GEOTHERMAL WELL RESULTS

4.1 Molecular Ratios in Brine

Typical brine atomic or molecular ratios used in geothermal fields include Na/K, Cl/SO_4, Cl/B, HCO_3/SO_4, and B/Li. Table 7 shows an average of the molecular ratios of the discharges of the different wells at DSP. Regarding the Na/K atomic ratio, which signals a high temperature zone, there is a clear tendency for that ratio to rise as the wells move due East. This agrees well with the fact that SP05 and SP06 are drilled in the oldest dome, therefore the coolest region, but also are shallower with respect to SP01 and SP04.

The Cl/B ratio can be used in wells in a similar manner as in warm spring discharges, in that a similar ratio points to a common source reservoir. As has been discussed, though, caution is required as Boron differences can arise from a change in lithology or by adsorption of it into clays during lateral flow. This ratio decreases as the wells move due East, as shown in the data of Table 7. Nonetheless, it is believed that the ratio remains similar enough to point to a common reservoir. At the same time, studying the Boron tendency of the wells as shown in Table 3 it is seen that the concentration is lowest in SP06, suggesting lateral flow in this direction. An increase in the HCO_3/SO_4 ratio would indicate the well is away from the upflow zone, as this gives a greater opportunity for production of HCO_3 and oxidation of H_2S. For the wells producing at DSP, this ratio is greater on both wells drilled in the Eastern side of the domic complex, and highest in SP05, suggesting once again, that the lateral flow zone is located due East of DSP.

Finally, the B/Li ratio is used in a similar way as the Cl/B ratio to indicate flow direction, except it increases with flow. The information showed in Table 7 agrees with this, as the higher ratios are in wells SP05 and SP06. All these ratios point to a lateral flow zone existing towards the East of Domo San Pedro. Combining this with the highest concentrations of non-condensable gases in wells SP05 and SP06, as shown in Table 4 it's reasonable to assume that, while the western side of DSP (SP01 and SP04) is younger, and therefore hotter, the eastern side (SP05 and SP06) is located nearer the upflow and outflow of the system.

Table 7: Molecular Ratios of Brine in Production Well Discharges at DSP

Well	Na/K	Cl/B	HCO3/SO4	B/Li
SP01	3.6	10.5	1.0	2.0
SP04	3.9	9.9	3.5	2.1
SP05	4.5	9.6	3.2	2.8
SP06	8.6	8.8	1.8	4.0

4.2 Brine Geothermometers

Table 8 shows selected brine geothermometer estimates for production wells at DSP. As can be seen, most geothermometers shown agree quite well with the estimated formation temperatures of the wells. All the quartz geothermometers are below the estimated formation temperature, likely due to silica deposition during the trajectory the water makes from the reservoir to the well. The Na-K-Ca geothermometers all agree quite well with the formation temperatures, with the differences likely explained by uncertainties in the estimated formation temperature, or Na, K or Ca analysis. The Fournier 1979 Na/K geothermometer overestimates the temperatures of wells SP1, SP04 and SP05 by 25°C. The same goes for Na/K by Giggenbach (1988). The Na/K geothermometer by Árnorsson (1983) overestimates the temperatures the most. Interestingly, all geothermometers underestimate the SP06 stabilized temperature.

Table 8: Selected Brine Geothermometers for Production Wells at DSP

Well	Estimated Formation Temperature (°C)	Quartz Adiabatic (°C)	Na-K-Ca (°C)	Na/K Fournier1979 (°C)	Na/K Giggenbach 1988 (°C)	Na/K Árnorsson 1983 (°C)
SP01	344	300	330	361	363	380
SP04	317	279	310	349	352	363
SP05	299	256	291	330	335	337
SP06	260	232	245	256	269	243

4.3 Ternary Diagram of Brine from Wells Discharging at DSP.

Figure 3, Figure 4 and Figure 5 shown above, show the Cl-SO4-HCO3, Li-Cl-B and K-Na-Mg for the warm springs around DSP and the production wells. Figure 3 presents the Cl-SO_4-HCO_3 diagram for the Domo San Pedro production wells. It's clearly visible that all wells are currently discharging from mature waters with a very homogeneous composition, agreeing with the different molecular ratios already presented.

Figure 4 is the Li-Cl-B ternary diagram for the wells at DSP. By plotting in the same diagram, the relative concentrations of Lithium, Chlorides and Boron of wells and spring discharges, it's immediately evident that all the warm springs discharging around Domo San Pedro, with the exception of SI, originate from the reservoir from which the wells discharge. Nonetheless, wells SP01 and SP04 plot slightly closer to the Li vertex (due to a slightly higher relative presence of Li) than the rest of the wells and warm springs.

Figure 5 is the Na-K-Mg ternary diagram for the wells at DSP. As mentioned before, the warm springs extrapolate to approximate 260°C. However, not all the wells plot near this temperature, as shown below. Wells SP01 and SP04 plot beyond to the 340°C line, SP05 near the 340°C line and SP06 around 270°C. In the case of well SP01 this temperature is close to its observed downhole temperature of 344°C. For SP04, the downhole temperature was measured to be 317°C, so this ternary diagram is overestimating the temperature by some 30°C. A similar case is observed in SP05, where the downhole temperature was observed at 299°C, meaning this ternary diagram is overestimating its temperature by some 40°C. Finally, well SP06 has a measured downhole temperature of 260°C, agreeing quite well with the 265°C, where it plots in this diagram. These discrepancies could be explained by the presence of even hotter fluid surrounding the well, fluid which enters the well and is cooled slightly, but still retains the geothermometry "fingerprint" of its surroundings.

4.4 Molecular Ratios in Gases

According to Nicholson (2012), relative to early-formed steam, later-formed steam presents these characteristics.

- Lower gas concentrations
- Lower CO_2/H_2S ratios
- Lower CO_2/NH_3 ratios
- Lower H_2S/NH_3 ratios
- Higher CO_2/H_2 ratios.

Table 9 show that at total discharge conditions, wells SP01 and SP04 have the lowest weight percentage of gases, while SP05 and SP06 have the highest. This suggests that the latter two wells, located to the East of DSP are closer to the upflow zone. The trend is also supported by the aforementioned ratios in that wells SP05 and SP06 also contain the highest ratios relative to SP04 and SP01

Table 9: Molecular Ratios of Gases in Production Wells at Total Discharge at DSP

Well	wt%	CO2/H2S	CO2/NH3	H2S/NH3	CO2/H2	N2/Ar
SP01	0.356	7.9	-	-	150.6	38.7
SP04	0.37	10.9	3998.9	366.4	262.4	45.6
SP05	0.966	13.8	3393.9	851.4	118.1	50.8
SP06	1.171	16.2	5672.9	360.3	132.3	53.9

This table also shows the N_2/Ar ratios for the different geothermal wells. Given the average N_2/Ar of the different wells, it's clear that there is a meteoric component to all the wells. Well SP06 has the highest N_2/Ar ratio, probably because it's the newest well and is still discharging water supersaturated with air that was injected during the drilling

4.5 Ternary Diagram of Gases from Wells Discharging at DSP

Gas analysis for the production wells of DSP are presented in Table 4, and some molecular ratios presented in Table 9. Two distinct trends can be observed in the gas composition of the production wells. Wells located in the western part of the field, SP01 and SP04, have a lower gas composition than wells located to the eastern side, SP05 and SP06. Figure 6 shows a N2-CO2-Ar ternary diagram for the well gas chemistry. All wells have a low N2/Ar ratio, and therefore plot near the air-saturated water vertex, suggesting a rich meteoric component to their discharges. The farthest well from this trend is well SP04 which plots closer to a crustal component than the other wells.

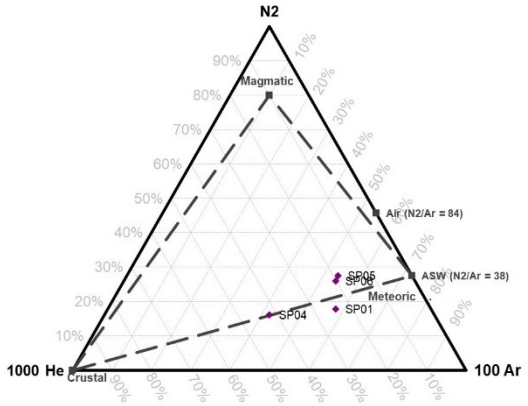

Figure 6: N2-He-Ar Ternary Diagram for Gases Discharging from Wells of DSP

4.6 Gas Geothermometers for Production Wells at DSP

Figure 7 show the CO2/Ar – H2/Ar geothermometer grid (CAR-HAR) with RH = -2.8. This geothermometer shows all wells are in equilibrium with fluid of around 225°C and 250°C. This estimate is a significant departure from the brine geothermometers discussed before, as most of them estimate temperatures closer to 300°C and upwards for the wells. The wells, by plotting between the equilibrated liquid and equilibrated vapor lines, suggest two-phase conditions in the subsurface. This has been corroborated with measurements of excess enthalpy in some production wells (not discussed in this paper).

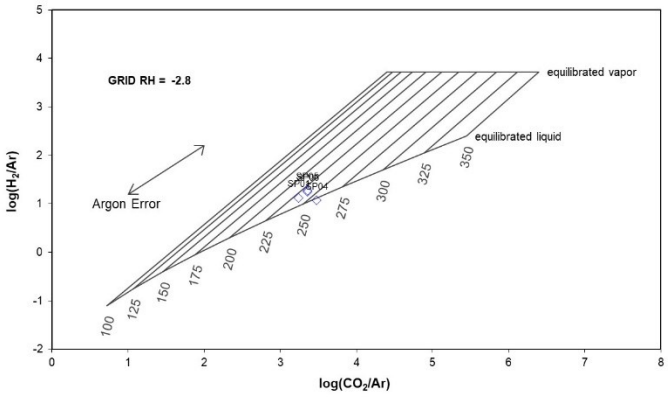

Figure 7: CO2/Ar - H2/Ar Geothermometer Grid

Figure 8 shows the FT-HSH geothermometer grid. Although mostly used for exploration geochemistry, this plot can still be used for estimated gas geothermometers on the discharges of production wells. As seen in this plot, this geothermometer overestimates the temperature significantly, plotting all wells above 350°C.

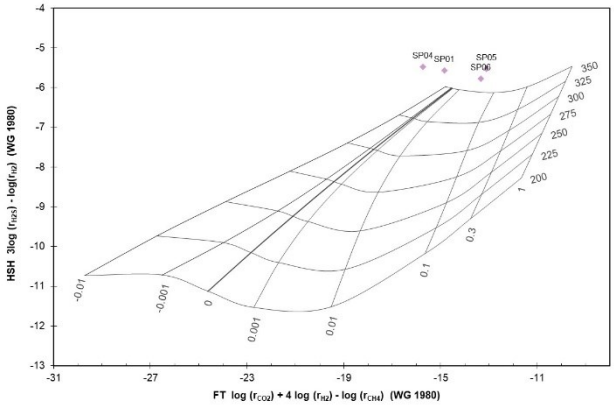

Figure 8: FT-HSH Geothermometer Grid for Production Wells at DSP

5. INTERPRETATION OF ISOTOPIC RESULTS

Figure 9 plots the isotopic results (Table 2) of all freshwater wells, precipitation, warm springs and geothermal production wells in the region around DSP. Meteoric lines have been plotted as rhombi, water bodies (rivers, lagoons, etc.) have been plotted as triangles, freshwater wells have been plotted as squares, and geothermal bodies (warm springs, production wells), have been plotted as circles. For simplicity, and to better represent the results, points LSP, RSP, LTT and LSM have been left out of the plot because they are located far relative to most points. These points correspond to 2 years of sampling, with most sampling points having at least two different analysis: one right before the start of the rainy season, and another just before the end of it.

The zones which are suspected to recharge the DSP reservoir are the RAM region and the Compostela region to the Southwest and West of the field, respectively. This relationship can be observed in the almost horizontal shift of the δ18O data.

The RAM samples have a slight Oxygen shift with respect to the local meteoric line because the river itself is does not originate where the sample was taken. These are waters that have precipitated, collected and transported mainly from the East for hundreds of kilometers. Nevertheless, the difference between transported and in situ water will be evaluated in the subsequent surveys, as a rain collector will be installed at this point. The recharge of the reservoir is facilitated in this location because at this location, the granodioritic unit which comprises the reservoir at DSP outcrops in a regional listric fault. This listric faulting favored the subsidence of this geologic unit towards the north, where it is found at DSP at an average depth of 300 m below sea level. The differences observed among the 3 samples taken at this point over the last 2 years respond to differences in wet/dry season. The input from this river to the geothermal reservoir is essential because this is a perennial river, with minor fluctuations depending on the time of year. This means it can continually supply recharge for the geothermal reservoir, almost guaranteeing the sustainability of the DSP field. It's also interesting to note that the dry-season sample from RAM is almost directly horizontal to the total discharge isotopic composition of the production wells. Comparing the RAM results with other samples directly horizontal from the production wells, namely RCH, ESP and UAN, RAM shows the smallest "oxygen shift" towards the production wells. The interpretation is that this system is close to stable, so that not even an extensive rock-water interaction will produce significant isotopic shift relative to the production wells.

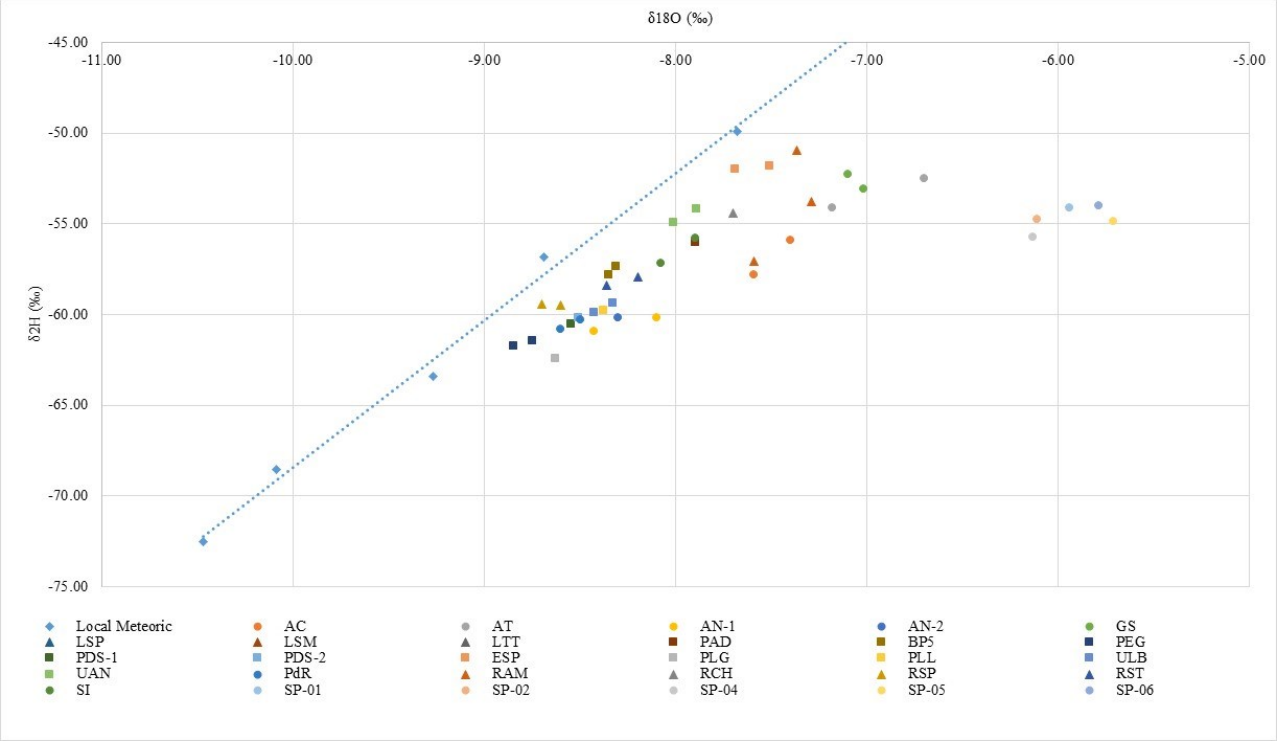

Figure 9: Isotopic Distribution of Wells, Warm Springs, Precipitation and Freshwater Wells around DSP

Another sample whose composition is similar to the production wells at DSP is RCH, with their δD composition averaging close to the DSP wells (around -54.5 ‰). For their δ18O content, the oxygen shift relative to the meteoric line is smaller than that of the RAM samples. The RCH river is part of a regional NW-SE fault that limits the Compostela graben to the south, which buries geologic units similar to that of those found in the geothermal reservoir. Therefore, any precipitation infiltrating along this fault will interact with rocks like the ones found in the reservoir. For this sampling point, only one analysis has been done (wet season 2017) because when attempting to sample during the height of dry season, the river was found dry. This means that this zone, and its recharge effect to the reservoir is seasonal.

The two other samples with similar δD to the production wells of DSP are UAN-1 and ESP-1. Both wells are in the Compostela graben above basalts and rhyolitic ignimbrite. Both samples have very small δ18O shift relative to the local meteoric line, associated with their meteoric origin and little residence time that does not allow lengthy rock-water interaction to enrich the water with 18O. Both freshwater wells were sampled during dry and wet season, and both plotted directly horizontal to the production wells. This means that regardless of seasonal precipitation, there is a shallow aquifer that permeates through all the lithological units and recharges the reservoir to some extent. During the structural campaign, a relevant fault, called CP Fault, was identified, which limits the Compostela Graben to the north. This fault buries rhyolitic units below basalts, so it is inferred that it extends to the geothermal reservoir.

Regarding warm springs, discharges from PdR, AN-1 and AN-2 are the most distant from the production wells at DSP from both δD and δ18O. Warm springs GS and AT average the same δD as the geothermal wells with a small (-1‰) oxygen shift, while AC plots between these two trends. Given how the δD of local precipitation is generally below the δD of the geothermal wells, the fact that PdR, AN-1 and AN-2 plot beneath the geothermal wells suggests these waters have been mixed with shallow aquifers recharged with rainwater.

A single isotopic point for the geothermal wells was calculated by knowing the average production of each well, their isotopic signature, and a weighted average calculation. The same was done for each warm spring and the local precipitation data. With this information, a mass balance was carried out for the percentage of cold water from RAM, RCH, UAN, ESP or rain water each spring possesses. Table 10 shows these results. Considering all sources of error, for both the silica mixing model and isotope mass balance, there is good agreement between the δ18O isotope mass balance and the Enthalpy-Silica Mixing Model.

Table 10: Estimated Parent Fluid Fraction using δ18O Balance

Warm Spring	Parent Fluid Fraction δ18O Balance	Best Freshwater Match δ18O Balance	Parent Fluid Fraction SiO2 Model
GS	17%	RAM	14%
PdR	17%	Rain water	6%
AT	26%	RAM	22%
AC	22%	UAN	30%
AN	25%	Rain water	21%

6. PRELIMINARY SUBSURFACE FLOWS AND GEOCHEMICAL MODEL

Considering the faulting system of the region, the chemistry of the brine and gas discharges of the geothermal wells, as well as the chemical and isotopic analysis of the warm springs and groundwater wells, a general subsurface flow and geochemical model is proposed.

In the DSP system, whose permeability is primarily controlled by structures and not porosity or permeability, it's reasonable to assume that the measured geologic faults, along with those inferred, can significantly control de outflow of the system. In this respect, Figure 10 shows the warm springs around the geothermal field (orange dots), the geothermal wells (red dots), fresh water wells (blue squares) and relevant rivers.

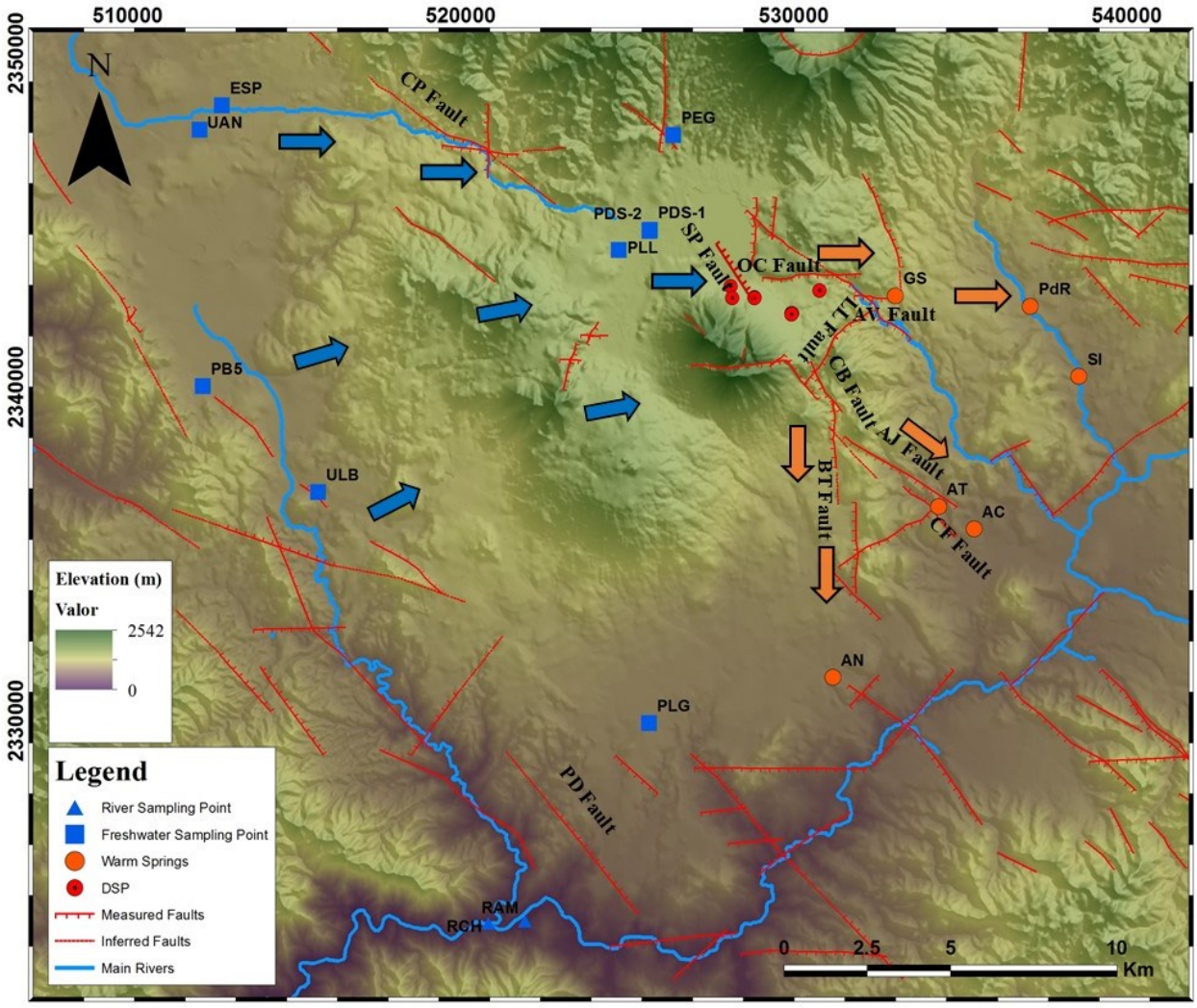

Figure 10: Regional Map with Observed and Inferred Faults

As shown, there is an inferred fault trending E-W which was observed in the Eastern flanks of the domic complex, near well SP05, which becomes a measured fault just South of GS, named AV Fault. South of this warm spring there are two NW-SE trending faults, which are named CB Fault and AJ Fault that continue to the SE, even reaching AC. However, in this same location, there seems to be another NE-SW (LL Fault) and N-S (BT Fault) which is inferred to reach as far south as AN. Finally, there is another measured fault trending NW-SE (CF Fault) at AT and AC which is inferred to be buried below the domic complex and resurface once again at the CP fault, some 8km NW of the field. From the information derived from the structural campaign, and geochemistry of wells and warm springs, we propose a general subsurface flow from the field towards the East in the direction of GS and PdR, along and parallel to OC Fault. Where it intersects the LL Fault, the flow begins a southern trajectory all the way to AN along BT Fault. Meanwhile, the fluid to the NW of the filed filters underground through CP Fault and reaches the surface at AT and AC via CB, AJ and CF Faults. The orange arrows of Figure 10 show the suggested outflow of the field. It's also possibly that some of the water flowing N-S through BT Fault towards AN changes direction towards the SE once it reaches CB Fault.

Given the isotopic results from freshwater wells and geothermal wells, it is believed the recharge zone of the field is the area directly to the West of the field. As has been discussed before, the ESP and UAN freshwater wells have a remarkably similar δD to that of the geothermal wells, suggesting a direct link between them. Also, there is an inferred fault that crosses this area in a NW-SE direction, which could aid the transport of rain (river) water from this area towards the heat source of the geothermal field.

Based on the geochemical information at hand that has been presented here, a geochemical model of the Domo San Pedro geothermal field is proposed and shown schematically in Figure 11.

The fluids have a meteoric origin, likely to the NW of the field, with some contribution of the region to the W and SW of the field. Little to no contribution of magmatic fluids is observed. Once these fluids reach the heat source beneath the domic complex, they form a liquid dominated reservoir with temperatures around 330°C and chloride concentration of 800-900 ppm. While moving W-E from wells SP01 and SP04 to SP05 and SP06, these fluids begin to boil possibly due to the small permeability encountered in the granodiorite and form a

small two-phase reservoir with lower temperature and slightly higher chlorides (900-1000 ppm). These fluids may also suffer from conductive cooling due to the slow movement of the water, also caused by the low permeability of the base rock.

The main upflow of the field is believed to be around wells SP05 and SP06, because these wells discharge the most gas, but probably closer to SP05 which is drilled closer to the domic complex than well SP06.

All the warm springs around the geothermal field have been diluted by freshwater but they still keep evidence in their molecular ratios and geothermometers of the original high temperature of the parent fluid. The measured and inferred faults of the region around the geothermal field suggest that the outflow initially begins to the East of the field, where it "turns" due South and Southeast to the AN and AT and AC warm springs, respectively.

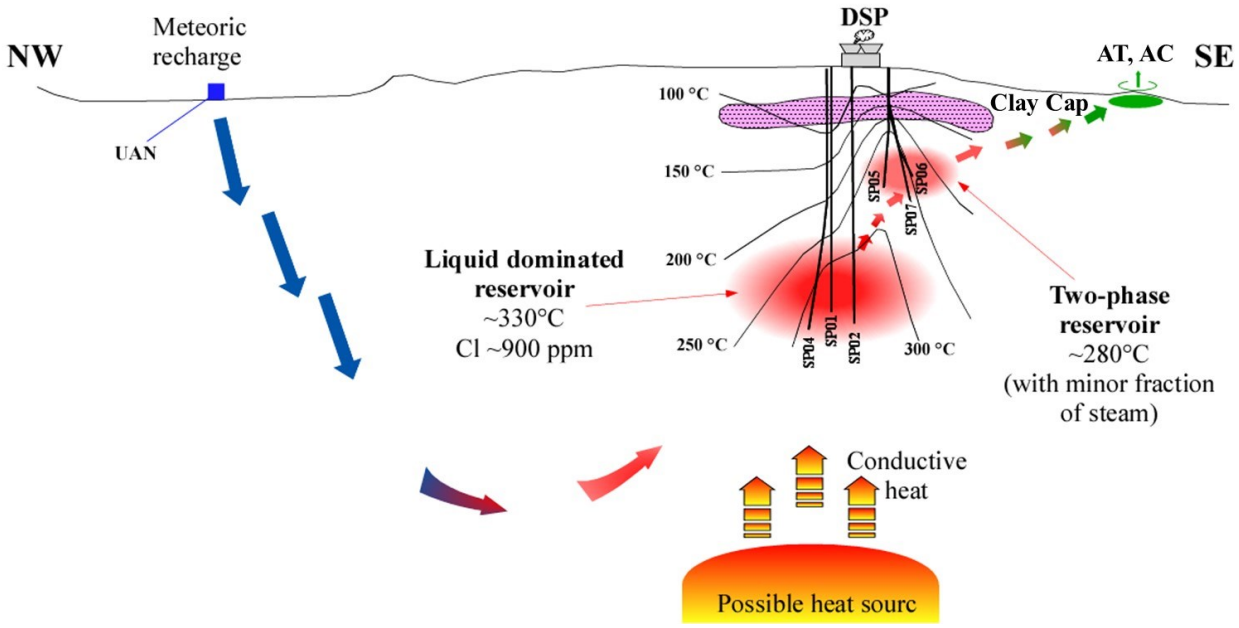

Figure 11: Geochemical Model of the Domo San Pedro Geothermal Field, Cross Section over CP, CB, CF Faults

7. ACKNOWLEDGEMENTS

The authors would like to thank the Grupo Dragon for their permission in publishing this paper.

REFERENCES

Ármannsson, H., and Ólafsson, M.: Geothermal Sampling and Analysis. 2nd Short Course on Surface Exploration of Geothermal Resources (2007)

Árnorsson, S: Chemical Equilibria in Icelandic Geothermal Systems: Implications for Chemical Geothermometry Investigations. *Geothermics,* **12,** (1983), 119-128.

Árnorsson, S., et al.: Sampling and Analysis of Geothermal Fluids. *Geofluids*, **6**, (2006), 203-206.

Fournier, R.: Chemical Geothermometers and Mixing Models for Geothermal Systems. *Geothermics,* **5** (1977) 41-50

Fournier, R.: A Revised Equation for the Na/K Geothermometer. *Geothermal Resources Council Transactions*, **3**, (1979), 221-224

Giggenbach, W. F.: Geothermal Solute Equilibria, Derivation of the Na-K-Mg-Ca Geoindicators. *Geochimica and Cosmochimica Acta*, **52,** (1988) 2749-2765.

Marini, L.: Geochemical Techniques for the Exploration and Exploitation of Geothermal Energy. Italy University, Genova (2000).

Nicholson, K.: Geothermal Fluids Chemistry and Exploration Techniques. Berlin. Springer (2012)

Powell, T., and Cumming, W.: Spreadsheets for Geothermal Water and Gas Geochemistry. *Proceedings,* 35th Workshop on Geothermal Reservoir Engineering, Stanford University, Stanford, CA. (2010)